*lubricants*

MDPI

*Article*

# Effect of Nanographene Water-Based Lubricant (NGWL) on Removal Behavior of Pure Copper

**Ziheng Wang [1], Zhenjing Duan [1], Shuaishuai Wang [1], Ji Tan [1], Peng Bian [1], Jiyu Liu [2], Jinlong Song [1] and Xin Liu [1,*]**

[1] State Key Laboratory of High-Performance Precision Manufacturing, Dalian University of Technology, Dalian 116024, China; wzh93123456@gmail.com (Z.W.); zhenjing456@126.com (Z.D.); wangshuais2022@126.com (S.W.); tanji20050125@mail.dlut.edu.cn (J.T.); bian_peng2023@163.com (P.B.); songjinlong@dlut.edu.cn (J.S.)

[2] College of Mechanical and Electrical Engineering, Northeast Forestry University, Harbin 150040, China; liujiyu19940802@163.com

* Correspondence: xinliu@dlut.edu.cn

**Abstract**

Pure copper is an important metal material in the fields of integrated circuits, mold manufacturing, and aerospace. Its excellent ductility and plasticity lead to problems such as burrs and tool wear in cutting, which poses great challenges to the improvement of machining accuracy and surface quality. To achieve high-quality and efficient processing of pure copper, this paper proposes to use nanographene water-based lubricant (NGWL) to regulate its removal behavior. A single-grain diamond scribing test and a micro-milling test were carried out to systematically study the action mechanism of NGWL on removal behavior of pure copper. The results showed that, compared with dry scribing at normal forces of 100, 400, 700, and 1000 mN, the material removal efficiency induced by NGWL was increased by 54.1%, 80.7%, 44.8%, and 30.3%, respectively. Compared with dry micro-milling at feed speeds of 200, 600, 1000, and 1400 μm/s, for the 75°XT4E tool, the surface roughness *Sa* with NGWL-assisted micro-milling was reduced by 75.5%, 73.1%, 61.4%, and 44.2%, respectively. Similarly, for the 65°UDT4E tool, compared to dry micro-milling, the *Sa* with NGWL lubrication was also reduced by 28.9%, 52.2%, 54.4%, and 36.9%, respectively. The *Sa* of pure copper induced by NGWL could be as low as about 20 nm without scales. Overall, NGWL can regulate removal behavior of pure copper by alleviating plastic deformation and promoting ductile fracture, thereby providing a new approach to achieving high-quality and efficient processing of pure copper.

**Keywords:** nanographene; pure copper; micro-milling; removal behavior; surface quality

check for updates

Received: 10 June 2025
Revised: 19 June 2025
Accepted: 24 June 2025
Published: 26 June 2025

**Citation:** Wang, Z.; Duan, Z.; Wang, S.; Tan, J.; Bian, P.; Liu, J.; Song, J.; Liu, X. Effect of Nanographene Water-Based Lubricant (NGWL) on Removal Behavior of Pure Copper. *Lubricants* **2025**, *13*, 286. https://doi.org/10.3390/lubricants13070286

**Copyright:** © 2025 by the authors. Licensee MDPI, Basel, Switzerland. This article is an open access article distributed under the terms and conditions of the Creative Commons Attribution (CC BY) license (https://creativecommons.org/licenses/by/4.0/).

## 1. Introduction

Pure copper is widely used in integrated circuits, mold manufacturing, aerospace, and other fields due to its excellent electrical and thermal conductivity [1–6]. Mold manufacturing is inseparable from high-speed cutting technology and electric discharge machining (EDM) technology [7–10]. As a commonly used electrode material for EDM, the processing accuracy and quality of pure copper directly determine the accuracy and quality of the mold. According to statistics, the cost of raw materials and processing of pure copper electrodes accounts for about 70% of the entire process cost [11], and the manufacturing of electrodes mainly relies on cutting. For some high-precision molds, the dimensional error is required to be less than 5 μm, and the surface roughness is lower than 0.025 μm [11–13].

However, the high ductility and plasticity of pure copper bring drastic plastic deformation and chip adhesion problems to processing. This causes the tool to wear easily and introduces plastic flow and burrs to the machined surface, which seriously affects the machining accuracy and surface quality. Therefore, it is of great significance to investigate removal behavior of pure copper in cutting to improve machining accuracy and quality.

The single-grain diamond scribing test is an important method to study removal behavior of materials [14–16]. Fu et al. [17] earlier investigated removal behavior of copper with different polishing fluids by scribing tests and found that the removal efficiency of copper with abrasive polishing fluids was much higher than that with deionized water. The reason was that abrasive polishing fluids could promote the formation of a softening layer in copper through chemical action. Wang et al. [18] established a crystal plasticity finite element simulation model of single crystal copper based on scribing tests. Both the experimental and the simulation results showed that dislocation slip was the main deformation mode in copper plastic deformation. Geng et al. [19] conducted scribing tests on single crystal copper using a double-tip probe and discovered that the dimensional parameters of the double-tip probe had a significant effect on normal force and scribed depth. Due to the symmetry of the double tips, the subsurface damage morphology on both sides of the tips also illustrated similarity. Zhu et al. [20] investigated the effects of scribing direction and scribing speed on the friction and wear behavior of single crystal copper and found that the wear of single crystal copper could be inhibited along the [110] direction and by increasing the scribing speed.

Micro-milling is a microscale machining technology with high flexibility and adaptability, which can achieve high-quality and efficient machining of tiny parts [21–23]. Gururaja et al. [24] introduced a machine learning algorithm in the process of micro-milling TC4 thin-walled parts. The trained support vector machine model could monitor and control the process parameters in real time to achieve adaptive machining of TC4 thin-walled parts. To predict the stability of high-speed micro-milling of AL7075, Chen et al. [25] established a micro-milling force model considering the nonlinear cutting coefficient and process damping effect. It was found that the cutting state was most stable at a spindle speed of 8000–70,000 rpm and a feed rate of 0.001–0.008 mm/tooth. In addition, minimum quantity lubrication (MQL) is widely used in cutting due to its green and environmentally friendly advantages [26–31]. Saha et al. [32] reported that MQL could significantly reduce the burr width and surface roughness of PMMA, and the best effect could be achieved when the cutting fluid flow rate was adapted to the spindle speed. Zhang et al. [33] combined biolubricants with MQL and proposed an enhanced MQL technology. They also revealed the cooling and lubrication enhancement mechanism of lubricants from the perspectives of molecular dynamics, fluid dynamics, and tribology. For pure copper materials, Filiz et al. [34] found in their study on micro-milling of pure copper that a lower feed rate would increase the wear rate of the tool, causing WC particles to fall off and creating more burrs on both sides of the groove. Büttner et al. [35] carried out a study on micro-milling of pure copper and tungsten copper using a milling tool with a diameter of 0.2 mm. The results indicated that, due to the high ductility of copper, there were problems such as groove burrs and tool wear, and the use of cutting fluid could significantly increase tool life. Therefore, it is of great significance to find a suitable processing method to regulate removal behavior of pure copper and achieve high-quality and efficient processing of it.

Due to the excellent heat dissipation capacity and lubrication properties of nanofluids [36], they have been widely used in the field of MQL-assisted cutting [37–42]. Yang et al. [43] claimed in a study of $MoS_2$ nanofluid MQL (NMQL)-assisted grinding of zirconia that, compared with dry and MQL-assisted grinding, the friction coefficient of NMQL-assisted grinding was reduced by 58.54% and 18%, respectively, and subsur-

face damage was suppressed. Duan et al. [44] combined cold plasma with NMQL and conducted micro-milling experiments on Al-Li alloys. The results implied that $Al_2O_3$ nanofluids could significantly reduce cutting forces, improve surface quality, and inhibit tool wear. Chu et al. [45] also found that nanoparticles could reduce the surface tension of the fluid and improve the permeability and heat dissipation capacity of the cutting fluid. Cui et al. [46] used carbon group nanolubricants such as fullerene, carbon nanotubes, and graphene to perform NMQL-assisted processing of aeronautical materials and found that carbon group nanolubricants could effectively improve the cooling and lubrication properties of the cutting interface and improve processing quality. Additionally, some studies also confirmed that nanographene has important application prospects in reducing friction and dissipating heat [47–50], which can effectively improve the machinability and surface quality of difficult-to-machine materials.

However, for pure copper, the effect and mechanism of nanographene water-based lubricant (NGWL) on its removal behavior have not been reported. In this paper, firstly, the scribing force, scribed morphology, and removal efficiency were measured and analyzed based on single-grain diamond scribing tests to reveal the effect of NGWL on removal behavior of pure copper. Then, the surface micromorphology and roughness, obtained by micro-milling tests, were employed to investigate the improvement of NGWL on machinability. This article provides a new approach to achieving high-quality and efficient processing of pure copper and a scientific reference for other difficult-to-machine materials.

## 2. Materials and Methods

### *2.1. Materials*

The material used in the test is pure copper, purchased from Anhui Zhengying Technology Co., Ltd. (Hefei, China), with the grade of TU1. Test samples with a size of 30 mm × 30 mm × 2 mm or 10 mm × 10 mm × 2 mm were obtained by cutting. The chemical composition and physical performance parameters of the materials are shown in Tables 1 and 2, respectively.

**Table 1.** The chemical composition content (wt%) of pure copper.

| **Elements** | Cu | P | Bi | Sb | As | Fe | Ni | Pb | Sn | S | Zn | O |
|---|---|---|---|---|---|---|---|---|---|---|---|---|
| **Content** | 99.97 | 0.002 | 0.001 | 0.002 | 0.002 | 0.004 | 0.002 | 0.003 | 0.002 | 0.004 | 0.003 | 0.002 |

**Table 2.** The physical performance parameters of pure copper.

| **Parameters** | **Unit** | **Value** |
|---|---|---|
| **Elastic modulus** | GPa | 128 |
| **Hardness** | HBS | 37 |
| **Yield strength** | MPa | 33.3 |
| **Tensile strength** | MPa | 209 |
| **Elongation** | | 60% |
| **Fracture toughness** | $MPa \cdot m^{1/2}$ | 30–50 |

NGWL is composed of 0.3 wt% few-layer nanographene (FLNG) powder and 99.7 wt% ethanol aqueous solution (ethanol concentration is 50%). FLNG was purchased from Shenzhen Suiheng Technology Co., Ltd. (Shenzhen, China). The number of layers is 1–3, the thickness is ~1 nm, and the particle size is 7–12 μm. The preparation process of NGWL is to mix FLNG and ethanol aqueous solution with a magnetic stirrer for 40 min and then put it into an ultrasonic cleaner with a power of 120 W for ultrasonic vibration for 1 h.

Finally, homogeneous and stable NGWL is obtained. Physical images of the preparation process are shown in Figure 1.




**Figure 1.** Physical images of the preparation process of NGWL.

### 2.2. Experimental Devices

As shown in Figure 2, the experimental devices mainly include a micro-milling machine and a single-grain diamond scribing device. The rotation accuracy of the micro-milling machine spindle (EMSF-3060K, Nakanishi, Tokyo, Japan) is within 1 μm, with a maximum rotation speed of 60,000 rpm. The feed accuracy of the feed platform (M-403, PI, Karlsruhe, Germany) can reach 0.2 μm. The maximum feed speed in the $x$, $y$, and $z$ directions is 10 mm/s. The Balzers nano-coated milling cutter (75°XT4E) and high aluminum titanium-coated milling cutter (65°UDT4E) used in the micro-milling test were purchased from Xiaorong Precision Tools (Shanghai) Co., Ltd. (Shanghai, China), and the milling cutter diameter is 1 mm. The lubrication method applied in the micro-milling test is atomization lubrication, and the nozzle model is YS-BPV-3000. The flow rate of NGWL is 40 mL/h. The single-grain diamond scribing device (Micro/nano-Scratcher-1000-V, Changchun, China) was developed by Jilin University [51]. The motion resolution in the $z$ direction of the scribing device is 5 nm, with a force resolution of 30 μN. It can achieve precise scribing of materials under a large force range of 1–1000 mN and a speed range of 1–100 μm/s. The cross-blade size of the diamond indenter (HV-6 Vickers indenter) used in the scribing test is 500 nm, and scribing is performed with the edge facing forward.

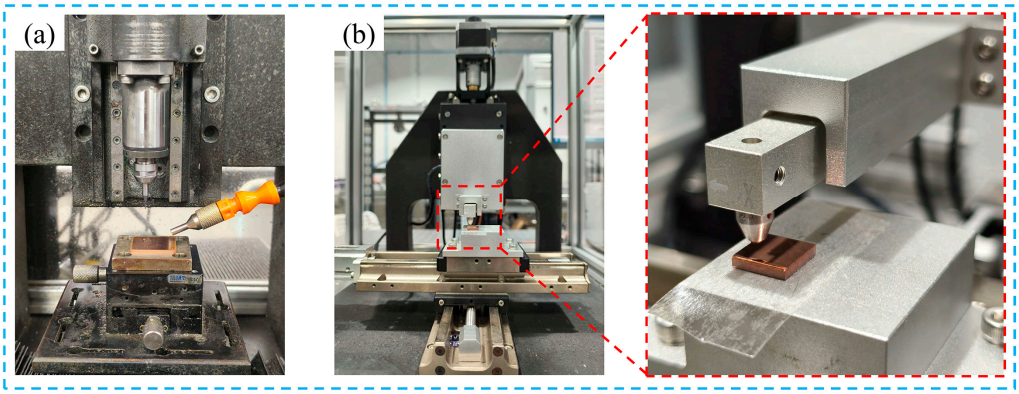



**Figure 2.** Experimental devices. (**a**) Micro-milling machine, (**b**) Single-grain diamond scribing device.

### 2.3. Characterization Methods

To reveal the mechanism of NGWL on removal behavior of pure copper, scribing tests were carried out on samples with and without NGWL lubrication using a single-

grain diamond scribing device. The scribed morphology, scribed depth, and material removal efficiency were measured and calculated by laser scanning confocal microscopy (LSCM) (LEXT OLS5100, Olympus, Tokyo, Japan) and scanning electron microscopy (SEM) (SEM5000, CIQTEK Co., Ltd., Hefei, China) [52–54]. After the micro-milling process was completed, the surface roughness and micromorphology were measured and analyzed using a 3D optical surface profiler (NewView9000, Zygo, Middlefield, CT, USA) and SEM.

## 3. Results

### *3.1. Single-Grain Diamond Scribing Experiment*

To explore the effect of NGWL on removal behavior of pure copper, variable force and constant force scribing tests were carried out on pure copper using a single-grain diamond scribing device. The scribing parameters used in the scribing test are shown in Table 3, and the scribing speed of all tests is 5 μm/s. A polished 10 mm × 10 mm × 2 mm copper sheet was used for the scribing test to avoid the influence of surface roughness on the test. The surface roughness *Sa* was about 8 nm. After the scribing test was completed, the scribing force–time curve and the scribed morphology were characterized. Meanwhile, to compare differences in the residual depth and material removal efficiency under conditions with and without NGWL lubrication, they were measured and calculated using the analysis software (version 2.2.2.251) provided by LSCM.

**Table 3.** Scribing parameters of the single-grain diamond scribing experiment.

| Experiment | Scribing Mode | Normal Force | Scribing Length |
|---|---|---|---|
| Exp. 1 | Variable-force | 0–1000 mN | 500 μm |
| Exp. 2 | Constant-force | 100 mN | 100 μm |
| Exp. 3 | Constant-force | 400 mN | 100 μm |
| Exp. 4 | Constant-force | 700 mN | 100 μm |
| Exp. 5 | Constant-force | 1000 mN | 100 μm |

#### 3.1.1. Variable-Force Scribing

Under conditions with or without NGWL lubrication, the scribing parameters shown in Exp. 1 in Table 3 were used to carry out a variable-force scribing test on pure copper, and the loading rate of normal force was 10 mN/s. The force–time curve and scribed micromorphology obtained by variable-force scribing are shown in Figure 3. $F_N$ and $F_L$ represent the normal force and the lateral force, respectively. As illustrated in Figure 3a,b, with the linear loading of $F_N$, the overall $F_L$ also showed a linear increase and fluctuations. Related studies have shown that fluctuation in $F_L$ is mainly related to the material fracture [55,56]. Obviously, the fluctuation degree of $F_L$ in Figure 3b was more severe than that in Figure 3a. This indicated that, after NGWL lubrication, removal behavior of pure copper was improved, which promoted material fracture. To further observe the fracture phenomenon during pure copper scribing, the scribed micromorphologies corresponding to positions 1, 2, 3, and 4 of $F_L$ were measured, as shown in Figure 3c,d. For the single-grain diamond scribing test, with a linear loading of $F_N$, the material will gradually go through three stages: sliding, plowing, and cutting. Observing the micromorphologies in Figure 3c,d, it could be seen that pure copper had entered the cutting removal stage. This was because the loading rate of $F_N$ used in the variable-force scribing was 10 mN/s, and the larger loading rate greatly shortened the durations of the sliding and plowing stages. Meanwhile, the width of the groove caused by scribing gradually increased with the loading of $F_N$, and there was plastic accumulation and material fracture on both sides of the groove. Compared with dry scribing, which only generated ductile fracture at position 2, the groove edge under NGWL lubrication showed ductile fracture at positions 1, 3, and 4. It also corresponded to

fluctuation in the lateral force. Due to the excellent ductility and plasticity of pure copper, it was difficult to fracture during cutting. Therefore, it was very easy to cause problems such as sticking and burrs, resulting in poor surface quality. The results of the variable-force scribing test demonstrated that NGWL could promote ductile fracture of pure copper, so it was expected to inhibit sticking and burrs during cutting and improve surface quality.

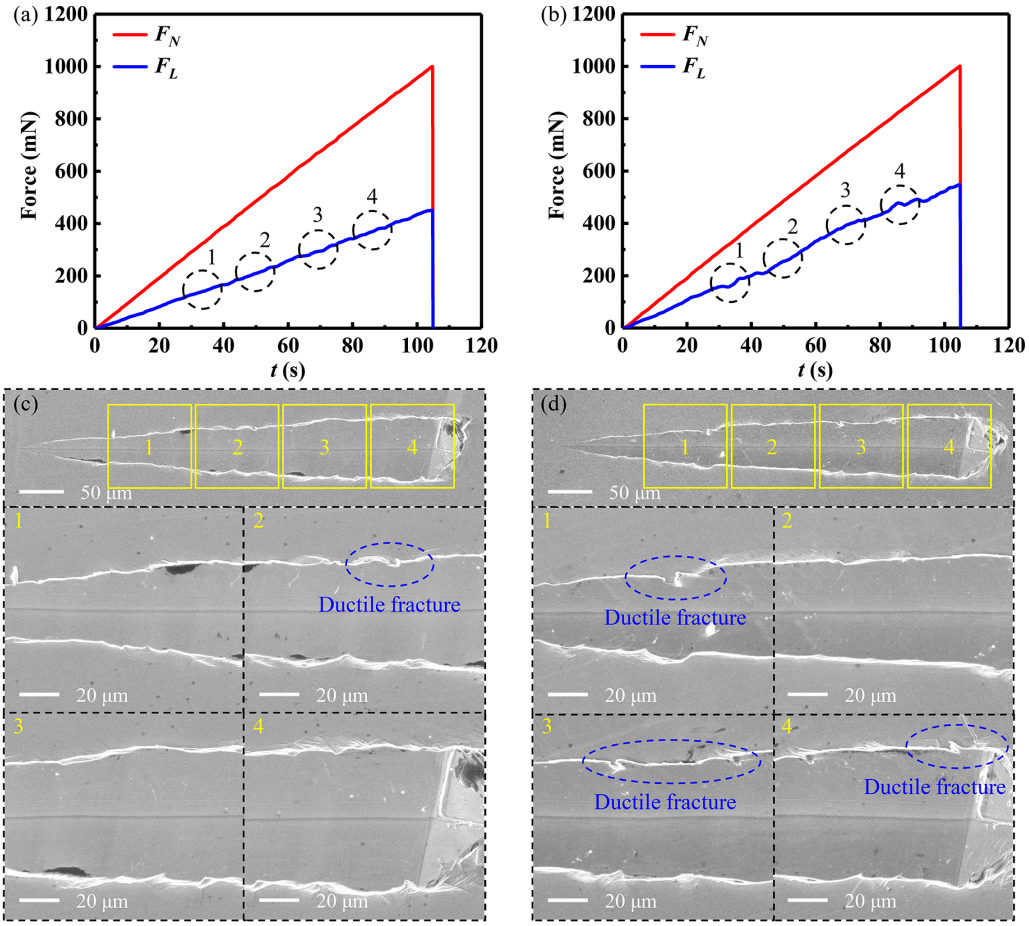



**Figure 3.** Force–time curves and scribed micromorphologies obtained by variable-force scribing of pure copper. (**a**,**c**) Dry, (**b**,**d**) NGWL.

### 3.1.2. Constant-Force Scribing

Based on the variable-force scribing test, the constant-force scribing test was conducted to further observe differences in removal behavior of pure copper under different lubrication conditions and different normal forces. The scribing parameters used in the test are shown in Exp. 2–Exp. 5 in Table 3, and the obtained scribed micromorphologies and 3D morphologies are shown in Figures 4 and 5. During the constant-force scribing process, a large amount of plastic strain will gradually accumulate at the scribed end, resulting in severe plastic deformation [57,58]. Slip is the main mechanism of plastic deformation of metal materials [59], so severe plastic deformation will stimulate a large amount of slip activity. Additionally, the scribing test was performed with the edge facing forward. The symmetry of the diamond indenter made the slip bands symmetrical as well, and finally formed the fishbone slip bands. Therefore, we regarded the fishbone slip bands as a sign of severe plastic deformation. When $F_N$ was 100 mN, no ductile fracture was observed on the scribed surface of pure copper, with or without NGWL lubrication. The reason might be that the normal force was small at this time, and the conditions for material fracture were not met. In addition, fishbone slip bands existed at the tail of the dry scribed groove, which were a trace of severe plastic deformation of the material (Figure 4a,e). When the

$F_N$ increased to 400 mN, fishbone slip bands also existed at the tail of the dry scribed groove, and the slip bands were denser than those at 100 mN. No fishbone slip bands were found at the tail of the groove assisted by NGWL, but ductile fractures were observed at its edge (Figure 4b,f). When the $F_N$ was further increased to 700 mN and 1000 mN, fishbone slip bands also existed at the tail of the groove under dry scribing, and there were a small number of ductile fractures (Figure 4c,d). After NGWL lubrication, there were multiple ductile fractures on the scribed surface, and no fishbone slip bands were found (Figure 4g,h). These phenomena indicated that NGWL could alleviate plastic deformation of pure copper and promote ductile fracture. Observing the 3D-scribed morphologies in Figure 5, as the scribing progressed, plastic accumulation of the material mainly occurred on both sides and in the tail of the groove. And under the same $F_N$, compared with dry scribing, plastic accumulation on both sides of the groove under NGWL-assisted scribing was weakened. These results indicated that NGWL could reduce plastic accumulation by alleviating plastic deformation of pure copper and promoting ductile fracture.

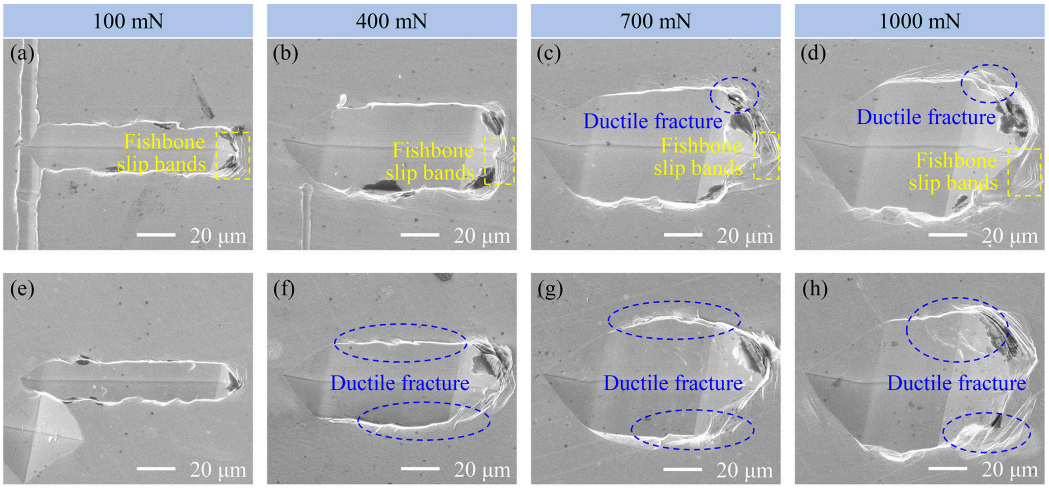



**Figure 4.** Scribed micromorphologies obtained by constant-force scribing of pure copper. (**a**–**d**) Dry, (**e**–**h**) NGWL.

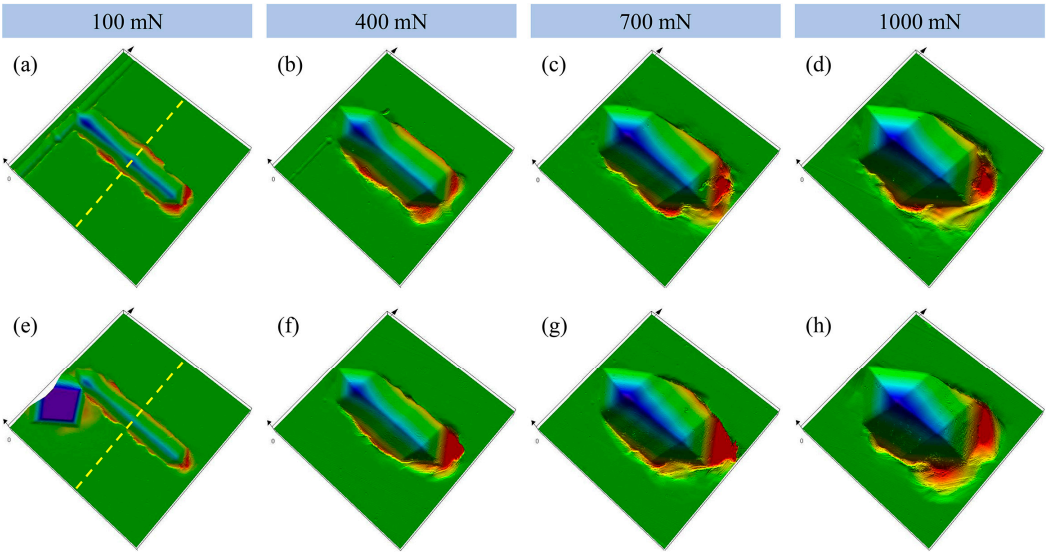



**Figure 5.** 3D micromorphologies obtained by constant-force scribing of pure copper. (**a**–**d**) Dry, (**e**–**h**) NGWL. (The yellow dotted line in the figure represents the measurement direction of the residual depth.)

The residual depth obtained by different forces was measured along the cross-sectional direction of the groove, and the results are shown in Figure 6. When $F_N$ = 100 mN, the plastic accumulation of dry scribing was higher than that of NGWL (Figure 6a), and the residual depth assisted by NGWL was lower than that of dry scribing. The reason might be that FLNG particles filled the microcracks and pores on the surface of pure copper during the scribing process, so that the diamond indenter scribed both pure copper and the filled FLNG particles at the same time, and the buffering effect of FLNG reduced the actual scribing depth of pure copper. When the $F_N$ increased to 400 mN and 700 mN, there was no obvious difference in the residual depth with or without NGWL lubrication, but the plastic accumulation on both sides of the groove under dry scribing was higher than that of NGWL (Figure 6b,c). When the $F_N$ reached a maximum value of 1000 mN, compared with dry scribing, the residual depth under NGWL-assisted scribing increased, and plastic accumulation on the side of the groove was suppressed (Figure 6d). The reason for the increase in depth was that NGWL could promote ductile fracture of pure copper, making it easier to remove at the same normal force.

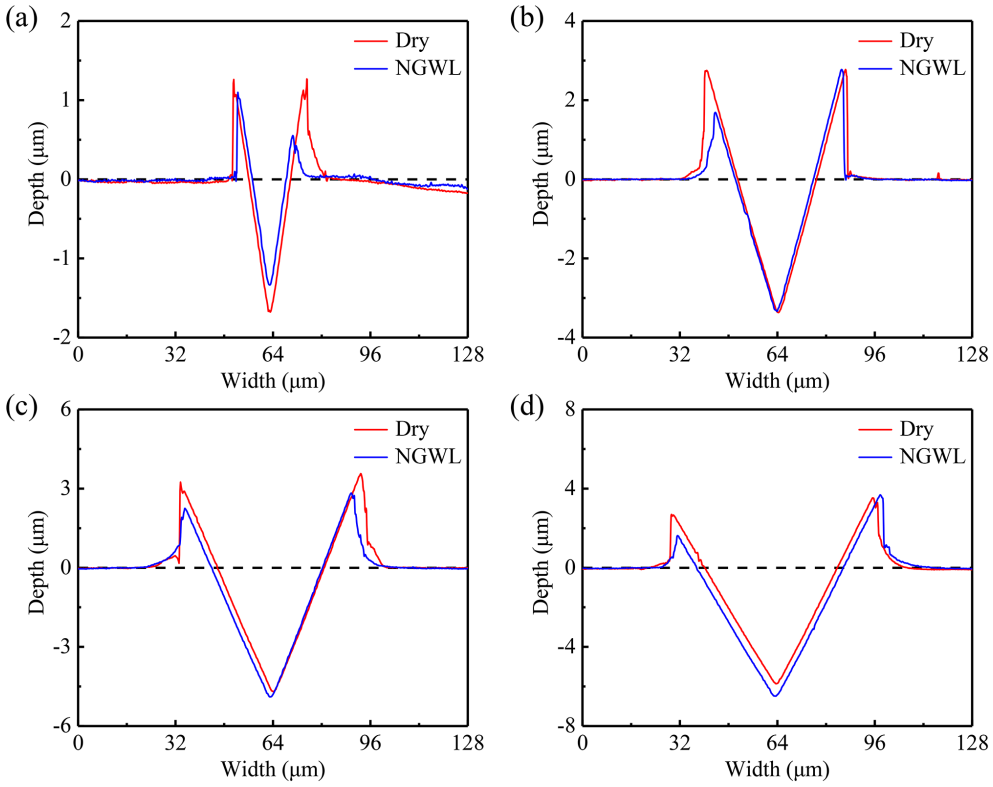



**Figure 6.** Residual depths at different normal forces. (**a**) 100 mN, (**b**) 400 mN, (**c**) 700 mN, (**d**) 1000 mN.

For the single-grain diamond scribing test, the cross-sectional area of the scribed groove affects material removal efficiency [60,61]. To further quantify the effect of NGWL on material removal efficiency, the total cross-sectional area of the groove was measured using the analysis software provided by LSCM. As shown in Figure 7a, the total cross-sectional area of the groove was the area enclosed by depth = 0 and the groove contour curve, which are the blue area $S_1$ and the purple area $S_2$ in the figure. $S_1$ is the area generated by the plastic accumulation of the material, and $S_2$ is the area generated by the actual scribing. Figure 7b,c demonstrate the areas $S_1$ and $S_2$ of dry and NGWL lubrication under different loads. Due to the serious plastic accumulation that occurred with dry scribing, the $S_1$ of dry scribing was higher than that of NGWL-assisted scribing. There was little difference in the area of $S_2$ with and without NGWL lubrication at 100, 400, and 700 mN. When the $F_N$ was 1000 mN, since NGWL could promote fracture of pure copper,

the $S_2$ obtained by NGWL was higher than that of dry. The calculation method of the material removal efficiency $R$ was as follows:

$$R = (S_2 - S_1)/S_2 \quad (1)$$

The $R$ value reflected the proportion of the area generated by plastic accumulation to the actual scribing area during the scribing process. That is, under the same conditions, smaller plastic accumulation corresponded to larger material removal efficiency $R$. The $R$ values with and without NGWL lubrication are shown in Figure 7d. Compared with dry scribing at an $F_N$ of 100, 400, 700, and 1000 mN, the $R$ value assisted by NGWL was increased by 54.1%, 80.7%, 44.8%, and 30.3%, respectively. Combined with the above analysis, it could be seen that NGWL could alleviate plastic deformation of pure copper to reduce plastic accumulation and promote fracture, thereby producing greater material removal efficiency under the same conditions.

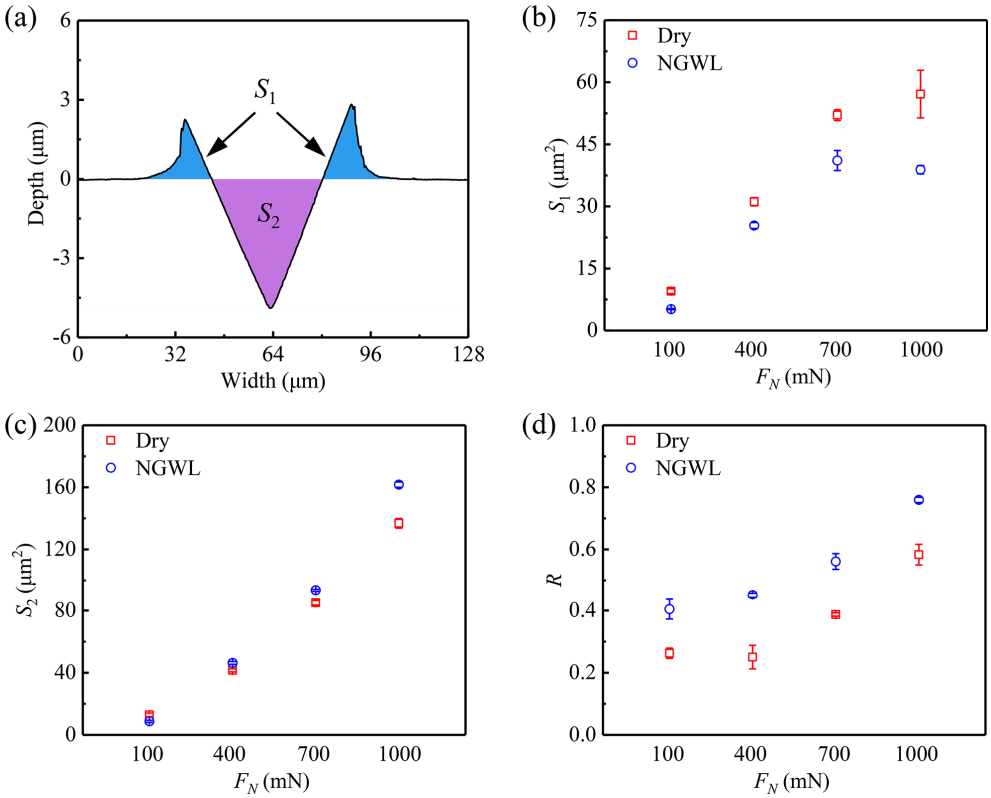



**Figure 7.** Groove cross-sectional areas $S_1$ and $S_2$ and material removal efficiency $R$ with and without NGWL lubrication at different normal forces. (**a**) Schematic diagram defining $S_1$ and $S_2$, (**b**) the area of $S_1$, (**c**) the area of $S_2$, (**d**) Material removal efficiency $R$.

### *3.2. NGWL Assisted Micro-Milling Experiment*

To explore the improvement effect of NGWL on the machinability of pure copper, micro-milling experiments were carried out using two different milling cutters (75°XT4E and 65°UDT4E) at spindle speed $n$ = 30,000 rpm, micro-milling depth $a_p$ = 3 μm, and feed speeds $V_f$ = 200, 600, 1000, and 1400 μm/s, and the machined surface roughness and micromorphology were measured and analyzed.

#### 3.2.1. Surface Roughness

For comparing the 3D morphology and roughness of the machined surfaces obtained under dry and NGWL conditions, they were measured using Zygo, and the measurement results are shown in Figure 8. For the 75°XT4E tool, when $V_f$ = 200 μm/s, the tool marks

under dry micro-milling were unevenly distributed. There were traces of material accumulation and local pulling on the machined surface, which was also called the scale phenomenon (Figure 8a). The scale phenomenon was mainly related to the chip adhesion and accumulation in the cutting of plastic metal materials and seriously limited improvement of surface quality. Pure copper would be squeezed by the tool during micro-milling, resulting in plastic deformation and accumulation. Its excellent ductility and plasticity made it difficult to fracture, thus causing the scale phenomenon. After the introduction of NGWL, the scale phenomenon on the machined surface was significantly alleviated, the tool marks were evenly distributed, and the surface quality was greatly improved (Figure 8e). When $V_f$ increased to 600, 1000, and 1400 μm/s, the scale phenomenon still existed on the machined surface under dry conditions (Figure 8b–d), which also showed that the scale phenomenon was not much related to the feed speed, but mainly to plastic deformation of the material. With the assistance of NGWL, the tool marks were evenly distributed, and no scale phenomenon occurred (Figure 8f–h). The results indicated that NGWL could alleviate adhesion and accumulation of the material by improving cooling and lubrication of the tool–workpiece interface, which in turn suppressed the scale phenomenon.

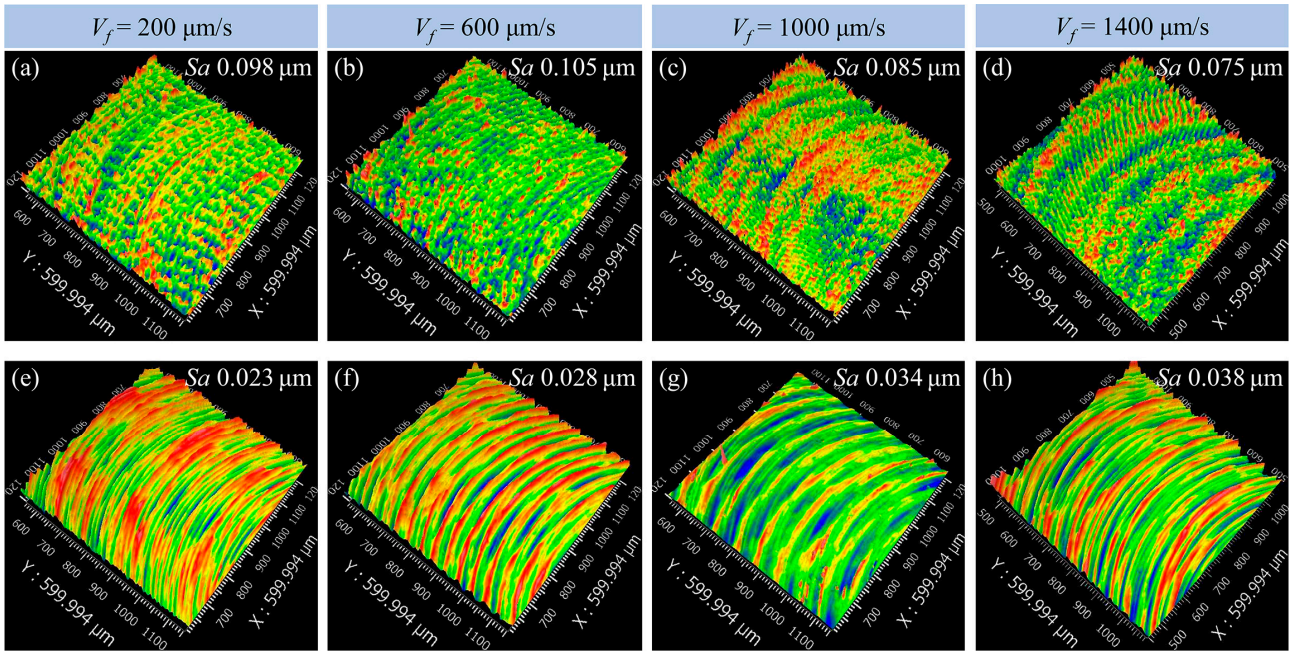



**Figure 8.** 3D morphologies of the machined surface obtained by the 75°XT4E tool under different lubrication conditions. (**a**–**d**) Dry, (**e**–**h**) NGWL.

For the 65°UDT4E tool, affected by the material plasticity, the tool marks of dry micro-milling at each feed speed were unevenly distributed. There was also a scale phenomenon on the machined surface (Figure 9a–d), but the scale phenomenon was alleviated compared with the 75°XT4E tool (Figure 8a–d). This also demonstrated that, compared with the Balzers nano-coated tool (75°XT4E), the high aluminum titanium-coated tool (65°UDT4E) was more suitable for processing pure copper. The reason was that, compared with the Balzers coating (TiAlN), the high aluminum titanium coating (AlTiN) had a higher Al content, and the chemical affinity of Al and Cu was less than that of Ti and Cu. This was attributed to Ti-Cu intermetallic compounds having a more negative Gibbs free energy [62,63] compared with Al-Cu intermetallic compounds, which made Ti and Cu have a stronger chemical affinity. Therefore, during micro-milling of pure copper, the Balzers coating tool was more susceptible to tool sticking, and diffusion reactions would occur to generate stable Ti-Cu intermetallic compounds. These increased tool wear and caused poor

surface quality. After using NGWL, the processing quality was significantly improved. The tool marks on the machined surface were evenly distributed, and there was no scale phenomenon (Figure 9e–h).

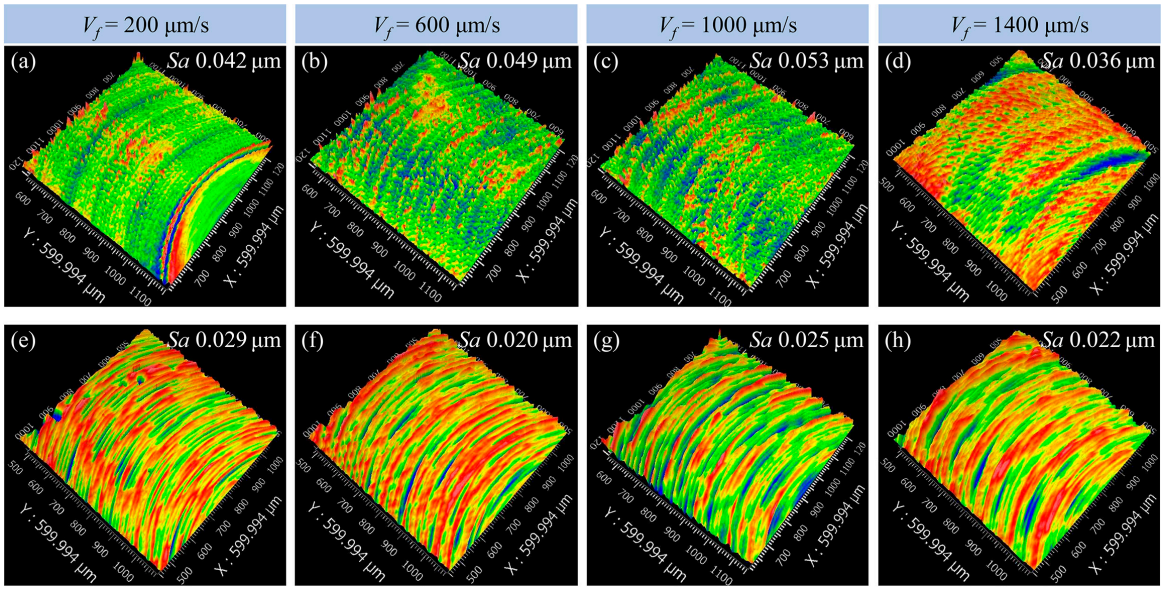



**Figure 9.** 3D morphologies of the machined surface obtained by the 65°UDT4E tool under different lubrication conditions. (**a**–**d**) Dry, (**e**–**h**) NGWL.

To quantitatively evaluate the surface quality obtained by different working conditions, the surface roughness of the two tools under different lubrication conditions was measured, and the results are shown in Figure 10. For dry micro-milling, with an increase in feed speed, the surface roughness *Sa* obtained by the 75°XT4E tool and the 65°UDT4E tool both showed a trend of first increasing and then decreasing. After the introduction of NGWL, with an increase in feed speed, the *Sa* obtained by the 75°XT4E tool also showed an increasing trend, while the *Sa* obtained by the 65°UDT4E tool was the largest at $V_f$ = 200 μm/s and then stabilized at about 0.022 μm. For the 75°XT4E tool, compared with dry micro-milling at $V_f$ =200, 600, 1000, and 1400 μm/s, the *Sa* with NGWL-assisted micro-milling was reduced by 75.5%, 73.1%, 61.4%, and 44.2%, respectively. Similarly, for the 65°UDT4E tool, compared to dry micro-milling, the *Sa* with NGWL lubrication was also reduced by 28.9%, 52.2%, 54.4%, and 36.9%, respectively. In addition, with dry micro-milling, the *Sa* obtained by the 65°UDT4E tool could be reduced by 58.8%, 58.4%, 42.5%, and 52.1%, respectively, compared with the 75°XT4E tool. This also indicated that the 65°UDT4E tool more easily obtained good surface quality when micro-milling pure copper.

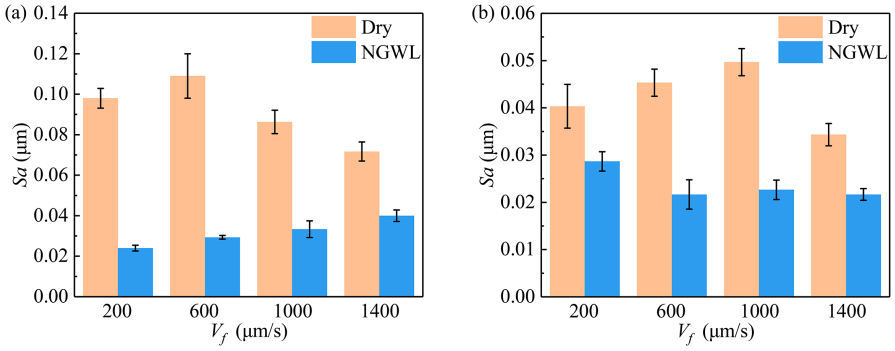



**Figure 10.** Surface roughness obtained under different lubrication conditions. (**a**) 75°XT4E tool, (**b**) 65°UDT4E tool.

### 3.2.2. Surface Micromorphology

On the basis of the above surface roughness measurement results, to further study the influence of different lubrication conditions on the processing quality of pure copper, the micromorphologies of the machined surface were measured using SEM. The measurement results are shown in Figures 11 and 12. For the 75°XT4E tool, due to the influence of material plastic deformation and accumulation, a large number of scales existed on the machined surface of dry micro-milling at each feed speed (Figure 11a–d). After the introduction of NGWL, scales also existed on the machined surface, but they were significantly suppressed compared with dry micro-milling (Figure 11e–h), which was also consistent with the previous 3D surface morphology results. Similarly, for the 65°UDT4E tool, scales also existed on the machined surface of dry micro-milling at each feed speed (Figure 12a–d), but they were reduced compared with the 75°XT4E tool with dry micro-milling. With NGWL lubrication, the scales basically disappeared, and the machined surface was smooth and flat (Figure 12e–h). Therefore, for two different tools, NGWL could improve cooling and lubrication of the tool–workpiece interface and improve surface quality.

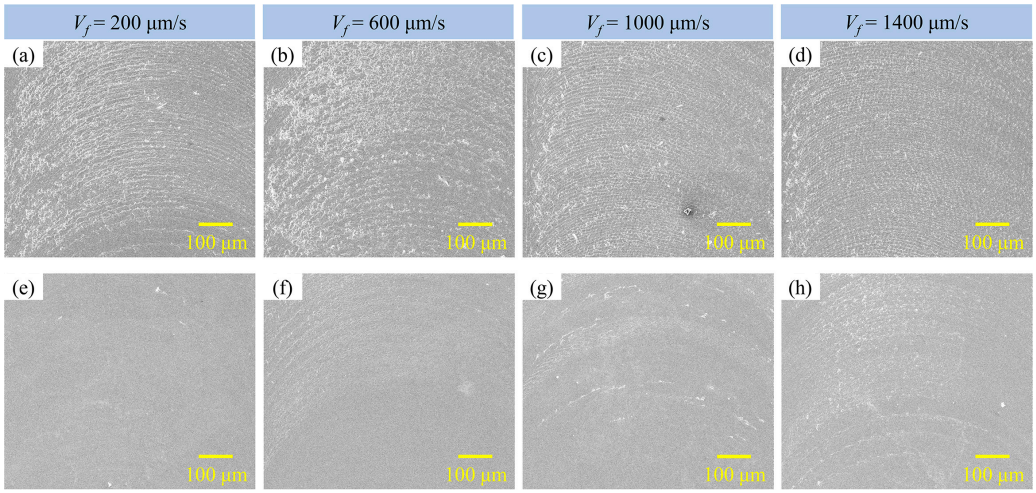



**Figure 11.** Micromorphologies of the machined surface obtained by the 75°XT4E tool under different lubrication conditions. (**a**–**d**) Dry, (**e**–**h**) NGWL.

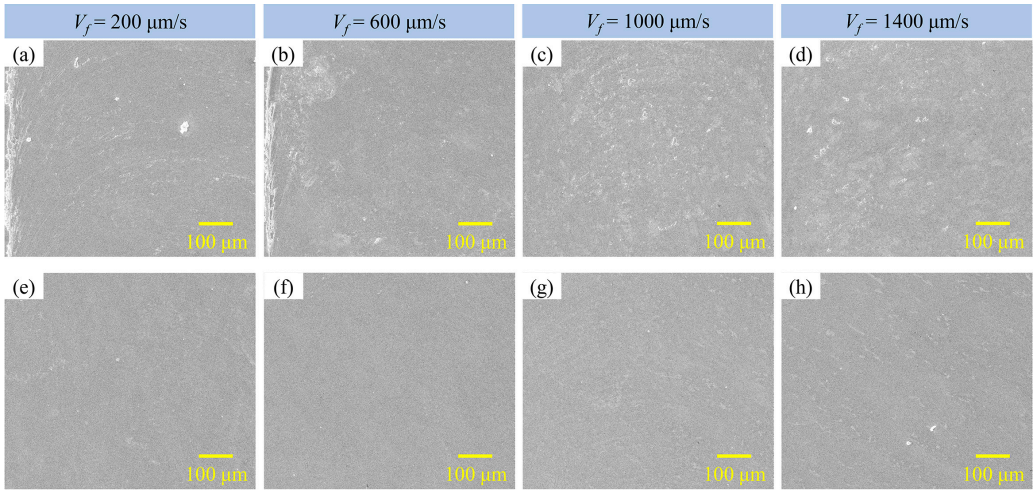



**Figure 12.** Micromorphologies of the machined surface obtained by the 65°UDT4E tool under different lubrication conditions. (**a**–**d**) Dry, (**e**–**h**) NGWL.

## 4. Discussion

According to the Rehbinder effect, highly chemically active nanoparticles can be adsorbed on the material surface and the crack tip, reducing their surface energy and thus promoting fracture [64,65]. Nanographene particles could penetrate into the grain boundaries of the cutting area, weaken the intercrystalline bonding force of pure copper through physical filling and chemical adsorption, and make the material easier to remove through ductile fracture. Meanwhile, the filling effect and directional arrangement of graphene nanoparticles could disperse stress concentration to a certain extent and reduce the severe plastic deformation caused by dislocation accumulation. Therefore, compared with dry scribing, the plastic deformation and accumulation of pure copper under NGWL-assisted scribing were alleviated, and ductile fracture was more likely to occur.

During micro-milling of pure copper, scales and tool marks were mainly related to plastic deformation and chip adhesion. The unique layered structure of graphene improved the lubrication properties of the tool–workpiece interface [49,50], reduced the friction coefficient and cutting force, and inhibited plastic deformation. Additionally, graphene filled the tool surface, forming an atomically smooth interface that protected the tool and reduced chip adhesion. The high thermal conductivity of graphene enabled it to quickly conduct localized heat in the cutting area, preventing the workpiece material from sticking to the tool due to softening. Hence, compared with dry micro-milling of pure copper, the surface quality of NGWL-assisted micro-milling was significantly improved, with an *Sa* as low as ~20 nm.

## 5. Conclusions

This paper proposed to use NGWL to regulate removal behavior of pure copper and systematically studied the action mechanism of NGWL on removal behavior of pure copper based on a single-grain diamond scribing test and a micro-milling test. The main conclusions of this paper are as follows:

(1) In the single-grain diamond scribing test, NGWL could alleviate the plastic deformation of pure copper, reduce plastic accumulation, and promote ductile fracture. Compared with dry scribing at $F_N$ values of 100, 400, 700, and 1000 mN, the material removal efficiency $R$ assisted by NGWL was increased by 54.1%, 80.7%, 44.8%, and 30.3%, respectively.

(2) Compared with dry micro-milling at $V_f$ values of 200, 600, 1000, and 1400 μm/s, for the 75°XT4E tool, the *Sa* with NGWL-assisted micro-milling was reduced by 75.5%, 73.1%, 61.4%, and 44.2%, respectively. Similarly, for the 65°UDT4E tool, compared to dry micro-milling, the *Sa* with NGWL lubrication was also reduced by 28.9%, 52.2%, 54.4%, and 36.9%, respectively.

(3) NGWL could reduce the plastic deformation caused by dislocation accumulation, thereby inhibiting the burr phenomenon in the cutting process and improving surface quality. After the introduction of NGWL, the surface roughness *Sa* of pure copper could be as low as about 20 nm, and there were no scales. This is of great significance for achieving high-quality and efficient processing of pure copper. Moreover, the stability of NGWL should be addressed in the future by methods such as nanographene wettability modification to realize its application in high-performance manufacturing.

**Author Contributions:** Conceptualization, Z.W.; methodology, Z.W.; validation, Z.D. and S.W.; formal analysis, J.T. and P.B.; investigation, Z.W., Z.D. and S.W.; data curation, Z.W. and Z.D.; writing—original draft preparation, Z.W.; writing—review and editing, Z.W., J.L. and J.S.; supervision, J.S. and X.L.; project administration, X.L.; funding acquisition, X.L. All authors have read and agreed to the published version of the manuscript.

**Funding:** This research was funded by National Natural Science Foundation of China (Grant No. 52475430), and the Fundamental Research Funds for the Central Universities (Grant No. DUT23YG118).

**Data Availability Statement:** The data presented in this study are available in the article; further inquiries can be directed to the corresponding author.

**Conflicts of Interest:** The authors declare no conflicts of interest.

## Abbreviations

The following abbreviations are used in this manuscript:

| | |
|---|---|
| EDM | Electric discharge machining |
| MQL | Minimum quantity lubrication |
| NMQL | Nanofluid minimum quantity lubrication |
| NGWL | Nanographene water-based lubricant |
| LSCM | Laser scanning confocal microscopy |
| SEM | Scanning electron microscopy |
| FLNG | Few-layer nanographene |
| $F_N$ | Normal force |
| $F_L$ | Lateral force |
| $R$ | Material removal efficiency |
| $n$ | Spindle speed |
| $a_p$ | Micro-milling depth |
| $V_f$ | Feed speed |
| $Sa$ | Surface roughness |

## References

1. Popescu, I.N.; Alhalaili, B.; Anghelina, F.V.; Nicolicescu, C.; Vidu, R. Tribological Behaviors and Statistical Experimental Design of Sintered and Age-Hardened Aluminum–Copper Based Composites. *Lubricants* **2025**, *13*, 172. [CrossRef]
2. Zheng, Y.; Niu, J.; Lu, Y.; Xu, S.; Li, Z.; Zhao, H.; La, P. High strength and high conductivity pure copper prepared by ECAP-Conform combined with cryogenic rolling and recrystallization annealing. *J. Mater. Res. Technol.* **2025**, *36*, 3192–3204. [CrossRef]
3. Avila-Salgado, D.A.; Juárez-Hernández, A.; Izaguirre-Bonilla, N.J.; Muñoz Tabora, J.; Camacho-Martínez, J.L. Evolution of Microstructure, Hardness, and Wear Behavior of Medium-Entropy CuNiSiCrCoTiNbx Alloy. *Lubricants* **2025**, *13*, 164. [CrossRef]
4. Goto, I.; Kurosawa, K.; Matsuki, T. Effect of 3D-printed sand molds on the soundness of pure copper castings in the vicinity of as-cast surfaces. *J. Manuf. Process.* **2022**, *77*, 329–338. [CrossRef]
5. Alaghmandfard, R.; Aghayar, Y.; Ester, D.; Mohammadi, M.; Borisoff, J.; Dotto, K. Sintering process optimization of the additively manufactured pure copper parts through the metal paste deposited process. *J. Alloys Compd.* **2024**, *1009*, 176932. [CrossRef]
6. Wei, Y.; Chen, G.; Xiao, Z.; Zhang, Y.; Zhou, Y.; Liu, X.; Li, W.; Xu, J. Microstructures and mechanical properties of pure copper manufactured by high-strength laser powder bed fusion. *Opt. Laser Technol.* **2025**, *182*, 112134. [CrossRef]
7. Fallböhmer, P.; Rodríguez, C.A.; Özel, T.; Altan, T. High-speed machining of cast iron and alloy steels for die and mold manufacturing. *J. Mater. Process. Technol.* **2000**, *98*, 104–115. [CrossRef]
8. Shi, J.; Shan, Z.; Yang, H.; Huang, J.; Dong, S. Experimental and modeling studies on thermal-mechanical coupling of frozen sand molds cutting based on coarse-grained discrete element method. *J. Clean. Prod.* **2025**, *500*, 145250. [CrossRef]
9. Li, K.; Huang, X.; Chen, Q.; Xu, G.; Xie, Z.; Wan, Y.; Gong, F. Flexible fabrication of optical glass micro-lens array by using contactless hot embossing process. *J. Manuf. Process.* **2020**, *57*, 469–476. [CrossRef]
10. Kitada, R.; Wang, Q.; Tsuetani, S.; Okada, A. Influence of surface roughness of die sinking EDM on mold releasability in compression molding of thermosetting phenol resin. *Procedia CIRP* **2022**, *113*, 238–243. [CrossRef]
11. Skiba, J.; Kulczyk, M.; Przybysz-Gloc, S.; Skorupska, M.; Kobus, M.; Nowak, K. Effect of microstructure refinement of pure copper on improving the performance of electrodes in electro discharge machining (EDM). *Sci. Rep.* **2023**, *13*, 16686. [CrossRef]
12. Mahshid, R.; Zhang, Y.; Hansen, H.N.; Slocum, A.H. Effect of mold compliance on dimensional variations of precision molded components in multi-cavity injection molding. *J. Manuf. Process.* **2021**, *67*, 12–22. [CrossRef]
13. Sinico, M.; Witvrouw, A.; Dewulf, W. Improving the surface quality of maraging 300 parts produced via laser powder bed fusion through powder distribution selection and optimized laser remelting. *J. Manuf. Process.* **2025**, *138*, 38–49. [CrossRef]

14. Li, X.; Bonilla, M.R.; Lu, M.; Huang, H. Atomistic understanding of ductile-to-brittle transition in single crystal Si and GaAs under nanoscratch. *Int. J. Mech. Sci.* **2024**, *282*, 109689. [CrossRef]
15. Wang, J.; Yan, Y.; Cui, H.; Liu, S.; Li, C.; Geng, Y. Towards understanding the mechanisms of material removal and deformation in GaAs during nanomilling. *J. Mater. Process. Technol.* **2025**, *337*, 118712. [CrossRef]
16. Wang, Z.; Duan, Z.; Wang, S.; Li, Y.; Liu, J.; Song, J.; Liu, X. Material Deformation and Damage Mechanism Based on In-Situ Plasma-Assisted Nanoscratch Test of Single Crystal Silicon. *Chin. J. Mech. Eng.* **2025**, *38*, 67. [CrossRef]
17. Fu, W.; Chen, C.A.; Huang, K.; Chang, Y. Material removal mechanism of Cu-CMP studied by nano-scratching under various environmental conditions. *Wear* **2012**, *278–279*, 87–93. [CrossRef]
18. Wang, Z.; Zhang, H.; Li, Z.; Li, G.; Zhang, J.; Zhang, J.; Hassan, H.U.; Yan, Y.; Hartmaier, A.; Sun, T. Crystal plasticity finite element simulation and experiment investigation of nanoscratching of single crystalline copper. *Wear* **2019**, *430–431*, 100–107. [CrossRef]
19. Geng, Y.; Jia, J.; Li, Z.; Liu, Y.; Wang, J.; Yan, Y.; Gan, Y. Modeling and experimental study of machining outcomes when conducting nanoscratching using dual-tip probe on single-crystal copper. *Int. J. Mech. Sci.* **2021**, *206*, 106649. [CrossRef]
20. Zhu, J.; Xiong, C.; Ma, L.; Zhou, Q.; Huang, Y.; Zhou, B.; Wang, J. Coupled effect of scratching direction and speed on nano-scratching behavior of single crystalline copper. *Tribol. Int.* **2020**, *150*, 106385. [CrossRef]
21. Câmara, M.A.; Rubio, J.; Abrao, A.M.; Davim, J.P. State of the Art on Micromilling of Materials, a Review. *J. Mater. Sci. Technol.* **2012**, *28*, 673–685. [CrossRef]
22. Wang, Z.; Li, Y.; Wang, S.; Duan, Z.; Cao, X.; Zhou, Y.; Liu, X.; Liu, J. Feasibility and mechanism of atmospheric pressure cold plasma jet (APCPJ) assisted micro-milling of bulk metallic glasses (BMGs). *Ceram. Int.* **2024**, *50*, 11094–11105. [CrossRef]
23. Duan, Z.; Wang, Z.; Wang, S.; Zhang, B.; Bian, P.; Li, Y.; Liu, J.; Song, J.; Li, C.; Liu, X. Tool wear in enhanced minimum quantity lubrication assisted milling: From mechanism to application. *Chin. J. Aeronaut.* **2025**, 103597. [CrossRef]
24. Gururaja, S.; Singh, K.K. Machine learning based assessment of audio signal features for chatter identification in high-speed micromilling of thin-walled TC4 alloy. *Precis. Eng.* **2025**, *94*, 820–840. [CrossRef]
25. Chen, Q.; Li, W.; Ren, Y.; Zhou, Z. 3D chatter stability of high-speed micromilling by considering nonlinear cutting coefficients, and process damping. *J. Manuf. Process.* **2020**, *57*, 552–565. [CrossRef]
26. Dambatta, Y.S.; Li, C.; Sayuti, M.; Sarhan, A.A.D.; Yang, M.; Li, B.; Chu, A.; Liu, M.; Zhang, Y.; Said, Z.; et al. Grindability Evaluation of Ultrasonic Assisted Grinding of Silicon Nitride Ceramic Using Minimum Quantity Lubrication Based $SiO_2$ Nanofluid. *Chin. J. Mech. Eng.* **2024**, *37*, 25. [CrossRef]
27. Gao, T.; Xu, P.; Wang, W.; Zhang, Y.; Xu, W.; Wang, Y.; An, Q.; Li, C. Force model of ultrasonic empowered minimum quantity lubrication grinding CFRP. *Int. J. Mech. Sci.* **2024**, *280*, 109522. [CrossRef]
28. Yang, M.; Ma, H.; Li, Z.; Hao, J.; Liu, M.; Cui, X.; Zhang, Y.; Zhou, Z.; Long, Y.; Li, C. Force model in electrostatic atomization minimum quantity lubrication milling GH4169 and performance evaluation. *Front. Mech. Eng.* **2024**, *19*, 28. [CrossRef]
29. Yao, X.; Zhang, F.; Zhang, S.; Zhang, J.; Liao, D.; Lei, X.; Wang, J.; Du, J. Effect of Bio-Based, Mixed Ester Lubricant in Minimum Quantity Lubrication on Tool Wear and Surface Integrity in Ultra-Precision Fly-Cutting of KDP Crystals. *Lubricants* **2025**, *13*, 156. [CrossRef]
30. Liu, M.; Li, C.; Jia, D.; Liu, X.; Zhang, Y.; Yang, M.; Cui, X.; Gao, T.; Dambatta, Y.S.; Li, R. Model of atomized droplets average particle size and verification of eco-friendly hybrid lubrication (CAMQL). *Friction* **2025**, *13*, 9440960. [CrossRef]
31. Gu, G.; Wang, D.; Wu, S.; Zhou, S.; Zhang, B. Research Status and Prospect of Ultrasonic Vibration and Minimum Quantity Lubrication Processing of Nickel-based Alloys. *Intell. Sustain. Manuf.* **2024**, *1*, 10006. [CrossRef]
32. Saha, S.; Deb, S.; Bandyopadhyay, P.P. An analytical approach to assess the variation of lubricant supply to the cutting tool during MQL assisted high speed micromilling. *J. Mater. Process. Technol.* **2020**, *285*, 116783. [CrossRef]
33. Zhang, Y.; Li, L.; Cui, X.; An, Q.; Xu, P.; Wang, W.; Jia, D.; Liu, M.; Dambatta, Y.S.; Li, C. Lubricant activity enhanced technologies for sustainable machining: Mechanisms and processability. *Chin. J. Aeronaut.* **2025**, *38*, 103203. [CrossRef]
34. Filiz, S.; Conley, C.M.; Wasserman, M.B.; Ozdoganlar, O.B. An experimental investigation of micro-machinability of copper 101 using tungsten carbide micro-endmills. *Int. J. Mach. Tools Manuf.* **2007**, *47*, 1088–1100. [CrossRef]
35. Büttner, H.; Vieira, G.; Hajri, M.; Vögtlin, M.; Kuster, F.; Stirnimann, J.; Wegener, K. A comparison between micro milling pure copper and tungsten reinforced copper for electrodes in EDM applications. *Precis. Eng.* **2019**, *60*, 326–339. [CrossRef]
36. Shi, Y.; Zhao, B.; Ding, W. Solid Additives to Increase the Service Life of Ceramic Cutting Tool: Methodology and Mechanism. *Intell. Sustain. Manuf.* **2024**, *1*, 10009. [CrossRef]
37. Liu, G.; Wang, J.; Zheng, J.; Ji, M.; Wang, X. An Experimental Study on Ultrasonic Vibration-Assisted Turning of Aluminum Alloy 6061 with Vegetable Oil-Based Nanofluid Minimum Quantity Lubrication. *Lubricants* **2023**, *11*, 470. [CrossRef]
38. Cui, X.; Li, C.; Yang, M.; Liu, M.; Gao, T.; Wang, X.; Said, Z.; Sharma, S.; Zhang, Y. Enhanced grindability and mechanism in the magnetic traction nanolubricant grinding of Ti-6Al-4 V. *Tribol. Int.* **2023**, *186*, 108603. [CrossRef]
39. Bian, P.; Duan, Z.; Jia, Y.; Wang, Z.; Wang, S.; Tan, J.; Zhou, Y.; Song, J.; Liu, X. Evaluation of Surface Integrity of Multi-Energy Field Coupling-Assisted Micro-Grinding Hastelloy Alloy. *Micromachines* **2025**, *16*, 565. [CrossRef]

40. Cui, X.; Li, C.; Zhang, Y.; Said, Z.; Debnath, S.; Sharma, S.; Ali, H.M.; Yang, M.; Gao, T.; Li, R. Grindability of titanium alloy using cryogenic nanolubricant minimum quantity lubrication. *J. Manuf. Process.* **2022**, *80*, 273–286. [CrossRef]
41. Gao, T.; Liu, J.; Sun, X.; Zhang, Y.; Yang, M.; Liu, M.; Xu, W.; An, Q.; Wang, D.; Xu, P.; et al. Enhanced permeation mechanism and tribological assessment of ultrasonic vibration nanolubricants grinding CFRP. *Tribol. Int.* **2025**, *204*, 110494. [CrossRef]
42. Cui, X.; Li, C.; Zhang, Y.; Ding, W.; An, Q.; Liu, B.; Li, H.N.; Said, Z.; Sharma, S.; Li, R.; et al. Comparative assessment of force, temperature, and wheel wear in sustainable grinding aerospace alloy using biolubricant. *Front. Mech. Eng.* **2022**, *18*, 3. [CrossRef]
43. Yang, M.; Hao, J.; Wu, W.; Li, Z.; Ma, Y.; Zhou, Z.; Gao, T.; Liu, M.; Cui, X.; Zhang, Y.; et al. Critical cutting thickness model considering subsurface damage of zirconia grinding and friction–wear performance evaluation applied in simulated oral environment. *Tribol. Int.* **2024**, *198*, 109881. [CrossRef]
44. Duan, Z.; Wang, S.; Li, C.; Wang, Z.; Bian, P.; Song, J.; Liu, X. Tribological and micro-milling performance of surfactant-free microwave plasma-modified $Al_2O_3$ nanoparticles biodegradable lubricants. *J. Clean. Prod.* **2025**, *493*, 144969. [CrossRef]
45. Chu, A.; Li, C.; Zhou, Z.; Liu, B.; Zhang, Y.; Yang, M.; Gao, T.; Liu, M.; Zhang, N.; Dambatta, Y.S.; et al. Nanofluids Minimal Quantity Lubrication Machining: From Mechanisms to Application. *Lubricants* **2023**, *11*, 422. [CrossRef]
46. Cui, X.; Li, C.; Ding, W.; Chen, Y.; Mao, C.; Xu, X.; Liu, B.; Wang, D.; Li, H.N.; Zhang, Y.; et al. Minimum quantity lubrication machining of aeronautical materials using carbon group nanolubricant: From mechanisms to application. *Chin. J. Aeronaut.* **2022**, *35*, 85–112. [CrossRef]
47. Xu, R.; Xue, Z.; Yang, D.; Li, X.; Nie, H.; Guo, Y.; Guo, H.; Yan, Q.; Gu, J. Highly Energy Release of Aluminum@Ammonium Perchlorate Composites Incorporated with Graphene Oxide-based Energetic Coordination Polymer. *Adv. Funct. Mater.* **2025**, *35*, 2423205. [CrossRef]
48. Shi, J.; Yin, S.; Li, H.; Yi, X.; Wu, H.; Cao, T.; Fan, X.; Liu, J.; Zhou, F. Operando formation of hydration layer and tribofilm of graphene oxide for achieving synergistic lubrication on electrochemical boronizing surface. *Carbon* **2025**, *235*, 120089. [CrossRef]
49. Almonti, D.; Salvi, D.; Ucciardello, N.; Vesco, S. Enhanced Wear Resistance and Thermal Dissipation of Copper–Graphene Composite Coatings via Pulsed Electrodeposition for Circuit Breaker Applications. *Materials* **2024**, *17*, 6017. [CrossRef]
50. Baiocco, G.; Salvi, D.; Ucciardello, N. Optimizing Graphene Nanoplatelet Coating for Enhanced Wear Resistance on Copper Through Electrophoretic Deposition Parameters. *J. Mater. Eng. Perform.* **2024**. [CrossRef]
51. Wu, H.; Huang, H.; Zhang, Z.; Yan, J. Micro-amplitude vibration-assisted scratching: A new method for one step and controllable fabrication of the microscale V-groove and nanoscale ripples. *Int. J. Extrem. Manuf.* **2025**, *7*, 035102. [CrossRef]
52. Chi, Y.; Dong, Z.; Cui, M.; Shan, C.; Xiong, Y.; Zhang, D.; Luo, M. Comparative study on machinability and surface integrity of γ-TiAl alloy in laser assisted milling. *J. Mater. Res. Technol.* **2024**, *33*, 3743–3755. [CrossRef]
53. Yan, D.; Lin, J.; Chen, Y.; Yang, X.; Lu, Y.; Song, J. High-Efficiency Water Collection of Superhydrophobic Condensation Absorber. *Adv. Sci.* **2025**, *12*, 2417024. [CrossRef]
54. Lv, S.; Liu, F.; Yang, Z.; Han, J.; Zhai, Y.; Mao, C.; Yan, D. Superhydrophobic surface with rice leaf structures fabricated by laser processing. *Opt. Laser Technol.* **2025**, *189*, 113072. [CrossRef]
55. Zan, Z.; Guo, K.; Sun, J.; Lu, Y.; Yang, B.; Jia, X.; Sivalingam, V.; Xi, J. Investigation on scratching force and material removal mechanism of 3D SiCf/C–SiC composites during single grain scratching. *J. Eur. Ceram. Soc.* **2022**, *42*, 5366–5379. [CrossRef]
56. Wang, Z.; Yang, W.; Duan, Z.; Wang, S.; Li, Y.; Zhou, Y.; Liu, J.; Song, J.; Liu, X. Experimental Study on Cold Plasma Jet (CPJ) Assisted Micro-Milling of 30CrMnSiNi2A. *Intell. Sustain. Manuf.* **2024**, *1*, 10017. [CrossRef]
57. Liu, W.; Jiang, B.; Lin, Q.; Wu, S.; Yang, R.; Wang, Z. Orientation-dependent plastic flow in nanoscratching of copper surfaces. *Wear* **2024**, *544–545*, 205316. [CrossRef]
58. Kareer, A.; Tarleton, E.; Hardie, C.; Hainsworth, S.V.; Wilkinson, A.J. Scratching the surface: Elastic rotations beneath nanoscratch and nanoindentation tests. *Acta Mater.* **2020**, *200*, 116–126. [CrossRef]
59. He, Q.; Yoshida, S.; Okajo, S.; Tanaka, M.; Tsuji, N. Characteristic dislocation slip behavior in polycrystalline HfNbTiZr refractory medium entropy alloy. *J. Mater. Sci. Technol.* **2025**, *210*, 29–39. [CrossRef]
60. He, Y.; Xiao, G.; Zhu, S.; Liu, G.; Liu, Z.; Deng, Z. Surface formation in laser-assisted grinding high-strength alloys. *Int. J. Mach. Tools Manuf.* **2023**, *186*, 104002. [CrossRef]
61. Duan, Z.; Wang, S.; Li, C.; Wang, Z.; Bian, P.; Sun, J.; Song, J.; Liu, X. Cold plasma and different nano-lubricants multi-energy field coupling-assisted micro-milling of Al-Li alloy 2195-T8 and flow rate optimization. *J. Manuf. Process.* **2024**, *127*, 218–237. [CrossRef]
62. Wei, Y.; Zhu, L.; Li, Y.; Chen, Y.; Guo, B. Formation mechanism and microstructure evolution of Cu/Ti diffusion bonding interface and its influence on joint properties. *Vacuum* **2023**, *213*, 112167. [CrossRef]
63. Wei, Y.; Li, J.; Xiong, J.; Zhang, F. Investigation of interdiffusion and intermetallic compounds in Al–Cu joint produced by continuous drive friction welding. *Eng. Sci. Technol.* **2016**, *19*, 90–95. [CrossRef]

64. Chaudhari, A.; Soh, Z.Y.; Wang, H.; Kumar, A.S. Rehbinder effect in ultraprecision machining of ductile materials. *Int. J. Mach. Tools Manuf.* **2018**, *133*, 47–60. [CrossRef]
65. Chaudhari, A.; Wang, H. Effect of surface-active media on chip formation in micromachining. *J. Mater. Process. Technol.* **2019**, *271*, 325–335. [CrossRef]

**Disclaimer/Publisher's Note:** The statements, opinions and data contained in all publications are solely those of the individual author(s) and contributor(s) and not of MDPI and/or the editor(s). MDPI and/or the editor(s) disclaim responsibility for any injury to people or property resulting from any ideas, methods, instructions or products referred to in the content.